Heterodyne Transient Vibrational SFG to Reveal Molecular Responses to Interfacial Charge Transfer

Yingmin Li[1], Bo Xiang[1], Wei Xiong[1,2,*]

[1] Materials Science and Engineering Program, University of California, San Diego, La Jolla, CA 92093

[2] Department of Chemistry & Biochemistry, University of California, San Diego, La Jolla, CA 92093

We demonstrate heterodyne detected transient vibrational sum frequency generation (VSFG) spectroscopy and use it to probe transient electric fields caused by interfacial charge transfer at organic semiconductor and metal interfaces. The static and transient VSFG spectra are composed of both non-resonant and molecular resonant responses. To further disentangle both contributions, we apply phase rotation to make the imaginary part of the spectra be purely molecular responses, and the real part of the spectra be dominated by non-resonant signals. By separating non-resonant and molecular signals, we can track their responses to the transient electric-fields at interfaces independently. This technique combined with the phase sensitivity gained by heterodyne detection, allows us to successfully identify three types of photoinduced dynamics at organic semiconductor/metal interfaces: coherent artifacts, optical excitations that do not lead to charge transfer, and direct charge transfers. The ability to separately follow the influence of built-in electric fields to interfacial molecules, regardless of strong non-resonant signals, will enable tracking of ultrafast charge dynamics with molecular specificities on molecular optoelectronics, photovoltaics, and solar materials.

Introduction

Interfacial charge transfer is ubiquitous in photovoltaics, optoelectronics, and solar materials[1–8]. Yet, the charge transfer processes often occur at hidden interfaces rather than on the top surface, which makes it difficult to study the transfer process using surface techniques, such as scanning tunneling microscopy (STM), atomic force microscopy (AFM), or photoemission spectroscopy. Second-order nonlinear optical spectroscopy, i.e., second harmonic generation (SHG) and vibrational sum-frequency generation (VSFG), provides an elegant approach to probe hidden interfaces[9–16]. Its sensitivity to hidden interfaces comes from the fact that second-order nonlinear optical susceptibility only exists at non-centrosymmetric media, such as interfaces, when quadrupole and magnetic dipole contributions are negligible. In particular, VSFG probes molecular vibrational modes, which further provides molecular specificities at hidden interfaces. Since it was first demonstrated, VSFG has been a powerhouse technique for providing molecular level knowledge of a variety of interfaces, including air/water interfaces, interfaces of materials, and biological membrane systems[17–20].

The sensitivity of SHG or VSFG to interfacial charges could come from changes of electronic structures upon charge transfer, or, more generally, the so-called electric-field-induced effect. Electric-field-induced effect was first observed on SHG by Bloembergen, who showed SHG intensity was modulated by applying electrical potential at interfaces[21]. This intensity modulation is because a strong DC electric field is added to the interfaces, which further enables a third order $\chi^{(3)}$ signal. Because the electric field is largely screened in the bulk, the $\chi^{(3)}$ signal reflects the existence of strong DC electric fields at interfaces. Since then, electric field-induced effects have been seen on air/liquid interfaces with ionic surfactants[22–29], and many prototype charge transfer materials[1,9,14,15]. In particular, transient electric-field-induced SHG has been demonstrated by X.Y. Zhu and co-workers[1], and static and transient electric-field-induced VSFG has been developed by Massari[9] and our group[15], respectively. These developments provide a suite of tools to probe charge accumulation and dynamics at hidden interfaces.

Compared to SHG, VSFG should, in-principle, have the advantage of being able to follow molecular responses during interfacial charge transfers, which can provide insights into the role of interfacial molecules in many molecular optoelectronics, photovoltaics, and solar cell devices. However, as shown in both Massari's and our group's previous works[9,15], the VSFG spectra of charge transfer interfaces are often composed of both non-resonant (NR) and molecular resonant responses, and because NR signal often dominates the spectra, extracting molecular responses becomes difficult. Techniques such as adding delay between infrared (IR) and upconversion pulses could mitigate the NR signal, but add complications to the temporal dynamics.

In this report, we describe a new way to separate the NR and resonant VSFG signals in transient HD VSFG measurements[30,31] of charge transfer interfaces[32], which enables separate dynamic analysis of both the NR signal and the molecular response during charge transfer events. This method is based on heterodyne detection, which measures both the phase and amplitude of the emitted VSFG signals. We focus on a prototype charge transfer system composed of P3HT and Au. These two materials undergo dipole rearrangements and create new interfacial bands, which also enables new direct charge transfer pathways at interfaces. However, the associated dynamics are somehow still complicated by NR background. Therefore, it serves as an ideal system to develop heterodyne transient electric-field-induced VSFG to extract previously unavailable knowledge on this model system.

Methods

Sample preparation

The P3HT/Au system is prepared by a spin coating method. Titanium layers, which serve as the adhesion layer, are first sputtered onto glass slides. Then, gold layers are deposited on top of the titanium with a thickness of 150 nm. The Au substrates are sonicated in acetone for 15 minutes followed by ozone cleaning for 20 minutes before using. Regioregular P3HT polymers (from REIKE metals) are dissolved in chloroform to obtain an 8 mg/ml solution, which is then spin coated onto the Au substrates using 1500 rpm spin speed. The P3HT/SiO_2/Au system is prepared followed the same procedure as P3HT/Au except using a different substrate, where a thin layer of SiO_2 is magnetron sputtered on the gold slice with the thickness of 50 nm.

Heterodyne transient VSFG spectroscopy

The heterodyne transient vibrational sum frequency generation (HD tr-VSFG) spectrometer is based on a transient VSFG spectrometer described in our previous publication[15], a detailed schematic of the setup is included in the supporting information (Figure S1). The light source is an ultrafast Ti: Sapphire regenerative amplifier (Astrella, Coherent), which outputs 790-nm pulses (~35 fs, ~6 W, 1 kHz). The 790-nm pulses are then split into two parts. The major part (~5 W) is sent into an optical parametric amplifier (TOPAS, LightConversion) to generate two tunable near-IR pulses, referred to as signal and idler pulses. The signal and idler pulses after the TOPAS are spatially and temporally overlapped onto a type I barium borate (BBO) crystal to generate a mid-IR beam at 3.3 μm (~7 μJ) through the difference frequency generation (DFG) process. The residual 790-nm beam after TOPAS is used to prepare an upconversion pulse by passing the beam through a home-built pulse shaper for near-IR that narrows the spectra of the residual 790-nm beam to 0.6 nm or 9.5 cm^{-1} at full-width at half maximum (FWHM), which determines the spectral resolution. The minor part of the 790-nm fundamental pulse (~1 W) serves as the pump beam, which passes through a variable-length delay line before hitting on the sample. The pump pulse is modulated by a shutter which is controlled by a homemade Labview program. The shutter is modulated to be on and off every 1s which gives the integration time of pump on/off spectra. The power of the pump beam is controlled by a waveplate and polarizer.

The VSFG probe signal is generated by overlapping the mid-IR beam and the 790-nm upconversion beam both spatially and temporally at the sample surface. The center wavelength of the mid-IR is tuned to 3.3 μm to be on resonance with the C-H vibrational modes of P3HT. The mid-IR beam and the 790-nm beam are focused by an f = 10 cm parabolic mirror. Both beams approach the sample at about a 60-degree angle relative to the surface normal. The signal is collected by another parabolic mirror and collimated. After the beams get collimated, a piece of 2-mm thick CaF_2 crystal is added on the IR path to generate a time delay between the IR pulse and the 790-nm pulse for local oscillator (LO) generation[33,34], where a transmission geometry is implemented. Since the 790 nm upconversion pulse is long in time domain, the delayed IR would still overlap with the upconversion to generate the local oscillator. Moreover, due to the phase matching condition, it is much easier to insert delay media in the IR path. The VSFG probe, along with the other two beams, are focused by a lens (f = 10 mm) onto a Y-cut quartz crystal to generate the LO for heterodyne detection. The LO and VSFG signals are collimated by another lens (f = 10 mm) then passed through short-band pass filters to remove any 790-nm residuals, and then enter the monochromator and charge-coupled device (CCD) camera (400 X 1,340, Andor). LO and VSFG signals interfere with each other at the CCD, generating the heterodyne VSFG signal. A pair of waveplates and polarizers is used in each beam path to control both the beam intensity and polarization. The polarization configuration is kept at SSP through the whole experiment (S – SFG signal, S – 790 nm upconversion, and P – IR). The optical pump beam HD tr-VSFG signal is sent prior to the VSFG pulse sequence to trigger charge

transfer. Typically, 1.4 μJ is used to pump the sample. For the transient dynamic analysis, the pump probe signal at each time step is obtained by taking the difference of VSFG spectra when the pump pulse is switched on and off. The time delay between pump and probe pulses are controlled by a computerized stage, which randomizes its position during each scan to remove the effects of systematic errors on the dynamic trace. Between each scan, a height checker is applied to make sure the sample is at about the same height (the variation is within 1 μm).

Data collection is done by home-made Labview programs and Andor-Solis software. Each data set takes 20 minutes to finish that is well within the phase stable period. All the spectra are first Fourier transformed from the frequency domain to the time domain, then window function filters are applied to remove the DC signal. An inverse Fourier transform is applied to get the interference fringes in frequency domain. The interference fringes of the samples are then phase referenced by the HD SFG signal from a flat, clean gold surface. The transient signal is obtained by taking the difference between VSFG spectra with pump on and off.

Results and Discussion

Static HD VSFG spectra of P3HT/Au interfaces and its non-resonance signal

Before discussing transient HD VSFG dynamics of the P3HT/Au system, we must first show the static HD VSFG spectra of P3HT/Au to examine the phase stability of our setup, the sample and spatial heterogeneity of spectral phase, and the phase of the NR signal. We tested the phase stability on both Au substrates and freshly-made P3HT/Au sample. We measured HD VSFG spectra at the same spot of samples multiple times to examine the relationship between the sample condition and phase stability. We found that the phase of our phase reference, bare Au slice, remained stable for at least half an hour (Fig. 1a). We also observed that the phase of the P3HT/Au samples would undergo a constant decreasing due to

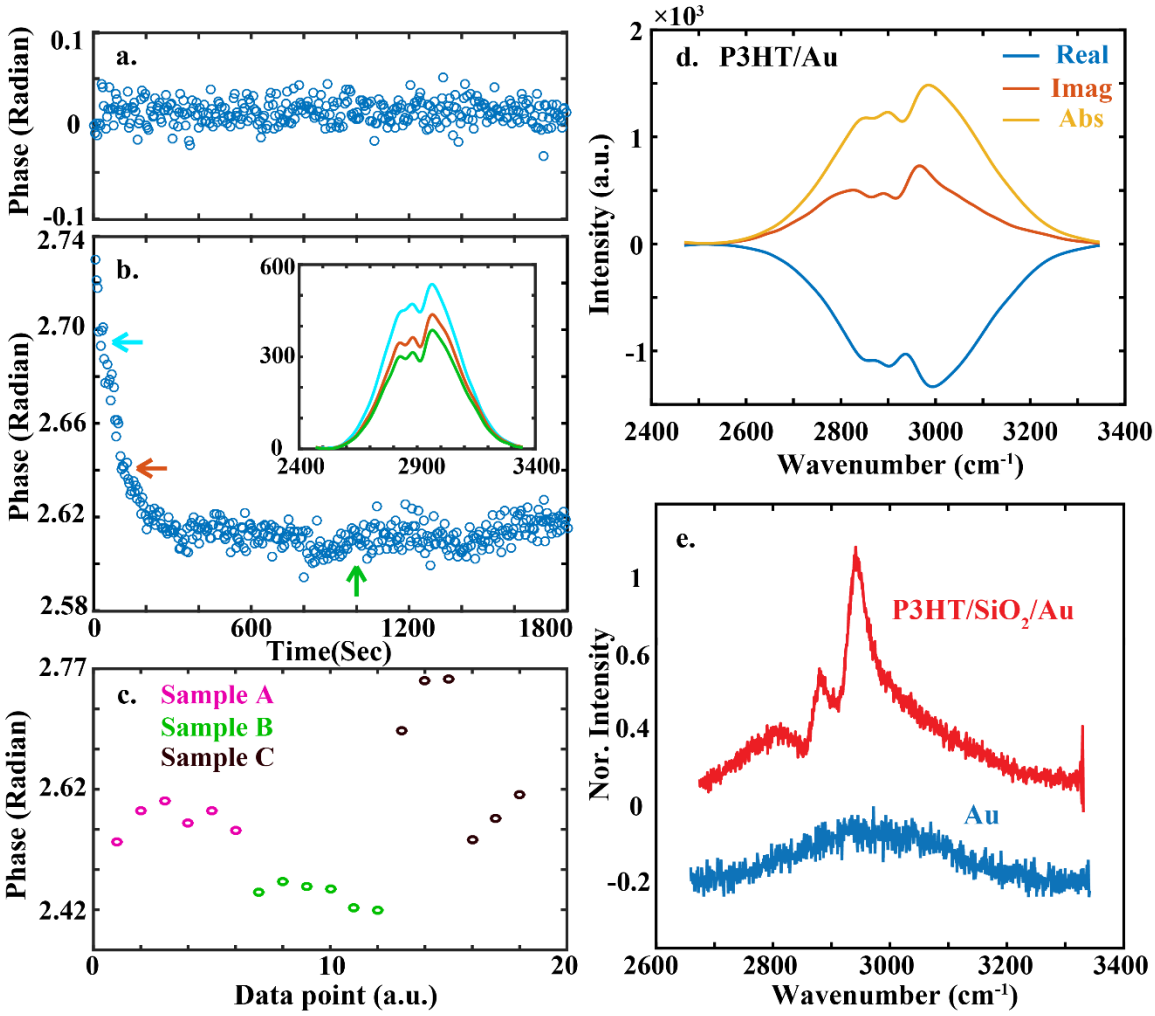

Figure 1. Phase stability and static VSFG spectra. (a) Phase stability of our phase reference, bare Au slide, in 30 minutes. The standard deviation is 0.0125. (b) Phase stability of P3HT/Au sample at the same spot. The inset shows three HD VSFG spectra of P3HT/Au at different times, as indicating by the arrows. Between the beginning of the scan (red) and the end of the scan (green), the spectra shape doesn't change. (c) Phase of three different P3HT/Au samples (A, B & C) prepared on three different days. Six different spots are tested for each sample. (d) Real, imaginary, and absolute HD SFG spectra of P3HT/Au sample. (e) Homodyne VSFG spectra of bare Au and P3HT/SiO_2/Au with very small non-resonant signal.

laser illumination before reaching an equilibrium state (Fig. 1b). However, the phase soon reaches a constant, and during the entire process, the lineshape and amplitude of VSFG spectra remain unchanged. Thus, we believe the initial phase drift is not due to sample damage, but rather to the light-induced annealing process, which is a subject for future studies. To guarantee consistency, all of our measurements are performed after the samples reach stable conditions. The phase of each measurement shows 0.02 radian variation within each measurement, which not only demonstrates the phase stability,

but also indicates that P3HT does not undergo sample degradation after reaching equilibrium, as the spectral phase is very sensitive to sample quality (Fig. 1b).

Next, we turn our attention to understanding whether there are spectral phase variations between different samples and different areas of the same sample. P3HT is a polymer and could be subject to spatial heterogeneities because of various molecular conformations at interfaces or subtle changes in sample preparation[35,36]. The result (Fig. 1c) suggests that different areas of the same sample do show some phase variations due to sample heterogeneity[36]. However, larger phase differences are seen between different samples because of various sample conditions. Therefore, the spectral analysis is conducted for each sample separately.

Lastly, we note that the HD VSFG spectra of P3HT/Au system have NR signals in both the real and imaginary parts of the spectra (Fig. 1d), indicating the phase of NR signal is not $\frac{\pi}{2}$ [37], as is the bare Au surface, instead, it's 2.69. In addition, all spectra are taken at SSP polarization, under which only a small NR signal appears for bare Au surface and P3HT/SiO_2 (Fig. 1e). All this evidence indicates that by depositing P3HT onto Au, the electronic bands of both materials hybridize and form new orbitals[38], which alters not only the phase but also the polarization selectivity of NR signals. The exact origin of these changes will be explored in future studies, in combination with theoretical works. Nevertheless, the existence of NR signals in both real and imaginary parts means that NR and molecular resonance signals are still mixed together, and, thus, imposes difficulties for following molecular specific dynamics, as we show in the next section. We also want to point out that the VSFG signal we observed comes from the buried interface as we discussed in our previous publication[15], where we showed the contribution from air/P3HT interface is almost negligible.

HD transient VSFG dynamics

The HD transient VSFG spectra are shown in Fig. 2a. From the transient spectra, we can clearly see that a time-dependent spectral shift exists in both real and imaginary parts of the dynamics where the spectrum centers at a higher wavenumber around time zero and shifts to a lower wavenumber at later time delay. To further understand the dynamics, we plot the integrated dynamics of both real and imaginary HD tr-VSFG spectra (Fig. 2b). The sign of the real part of the spectra is flipped for comparison purposes in both Fig. 2a and Fig. 2b. The dynamics of real and imaginary HD tr-VSFG spectra show similar overall dynamic features, where both spectrums have a negative peak around time zero, then the transient signals recover and become positive. However, it is obvious that the time scales associated with the real and imaginary spectral dynamics are different, which cannot be extracted if only the dynamics of homodyne VSFG is measured. For example, the recovery dynamics of imaginary spectral dynamics is slower than the real part.

Another way to analyze HD transient VSFG spectra is to plot the phase dynamics (Fig. 2c). Three cuts are taken at different frequencies: 2890 cm^{-1}, 2950 cm^{-1}, and 3050 cm^{-1}, as shown in Fig. 2d. Using Eq. 1, we can fit the dynamics cut at 2950 cm^{-1} into a combination of two exponential functions and a constant. We extract two components: a fast component, which decays in 120 fs, and another component that decays in around 1.14 ps. Therefore, the phase dynamics provide extra insights into the charge transfer process.

$$y = A_1 * e^{-t/\tau_1} + A_2 * e^{-t/\tau_2} + A_3 \quad \text{Equation 1.}$$

Yet, up to this point, it is still difficult to extract just the molecular dynamics involved in the charge transfer. This difficulty can be understood based on the Lorentzian model that is used for modeling VSFG

spectroscopy (Eq. 2). It can be easily expanded to show that unless the non-resonant phase φ is zero, both the real and imaginary components of the VSFG spectra contain NR and molecular resonant responses. However, NR and molecular resonance could have different temporal dynamics, which convolute all dynamics together and is the origin of the difficulty we encounter here.

$$\chi_{eff}^{(2)} = A_{NR} * e^{i\varphi} + \sum A_R * \frac{1}{(\omega+\omega_R)+i\Gamma} \quad \text{Equation 2.}$$

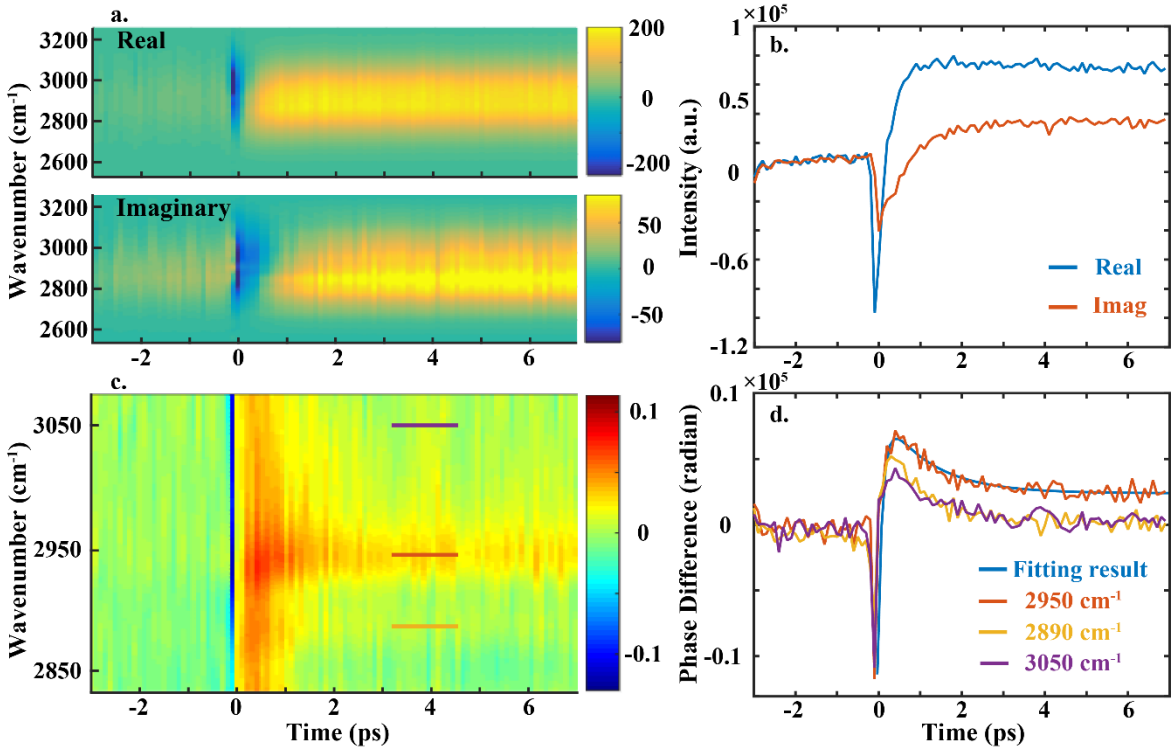

Figure 2. HD Transient-VSFG dynamics. (a) Pseudocolor 2D HD tr-VSFG spectrum of P3HT/Au sample. The upper panel shows the real part of HD dynamics, and the lower panel shows the imaginary part. (b) Integrated HD tr-VSFG dynamics for the real (blue) and imaginary (red) parts. The sign of the real-part spectra in both (a) and (b) is flipped for comparison purpose. Both parts show a negative signal at t=0, which recovers to a positive signal at t > 0. (c) 2D plot of the phase dynamics. The wavenumber axis is cut since the SNR of phase plot is low. Different color bar is applied from the 2D tr-VSFG spectra. (d) Cuts of phase dynamics at three different frequencies: 2890 cm^{-1} (orange), 2950 cm^{-1} (red) and 3050 cm^{-1}, as indicated by the colored lines in (c). The blue trace shows the fitting result of the cut at 2950 cm^{-1}.

Phase rotation to extract molecular dynamics

Fortunately, φ in Eq. 2 is a constant and independent of frequency. Thus, if φ can be determined, and a factor $e^{-i*\varphi}$ is multiplied to Eq.2, the NR signal can be shifted to the real component, and the molecular resonance will still have both real and imaginary components[32]. Most importantly, when the imaginary spectra are studied, they should only reflect molecular responses. The VSFG response after phase rotation is summarized in Eq. 3. Despite the function of the imaginary component appearing to be more complicated, the imaginary spectra can still be fitted using the same parameters of the original Lorentzian model for VSFG because φ is known.

$$\chi_{eff}^{(2)*} = \chi_{eff}^{(2)} * e^{-i\varphi} = A_{NR} + \sum A_R * \frac{1}{(\omega+\omega_R)+i\Gamma} * e^{-i\varphi} \quad \text{Equation 3.}$$

The phase φ can be determined by measuring the phase of HD VSFG spectra where there is no molecular resonance. This is a reasonable assumption, because although Lorentzian function has a long tail, NR signals often dominate the spectra, and, therefore, the spectra phase of HD VSFG is also dominated by the NR signal phase. In practice, we rotated the NR signal into negative real numbers, so it should have a phase of $\boldsymbol{\pi}$, which results in equation: $\boldsymbol{\varphi_{NR-PR} + \varphi = \pi}$, where $\boldsymbol{\varphi_{NR-PR}}$ is the phase of NR signal, $\boldsymbol{\varphi}$ is phase rotation factor. Thus, for the data of P3HT/Au, we determine φ to be 0.45 from the static HD VSFG spectra, for our following data analysis.

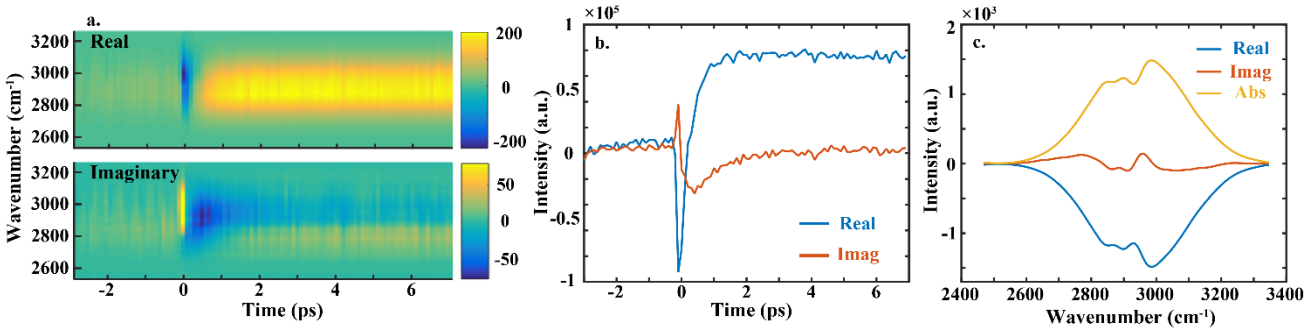

Figure 3. HD Transient-VSFG dynamics and static HD SFG spectra after phase rotation. (a) Pseudocolor 2D HD tr-VSFG spectrum of P3HT/Au sample after phase rotation. The upper panel shows the real part of HD dynamics, and the lower panel shows the imaginary part. (b) Integrated HD tr-VSFG dynamics for the real (blue) and imaginary (red) part after phase rotation. (c) The real (blue), imaginary (red), and absolute (yellow) static HD SFG spectra of P3HT/Au when not pumping the sample.

The phase-rotated HD VSFG spectra (Fig. 3c) show that NR signals are shifted to the real part of the spectra, whereas the molecular resonances appear in the imaginary spectra, as the imaginary spectra remain flat in the region where no molecular resonances are expected[39]. In the HD tr-VSFG spectra after phase rotation (Fig. 3a), it is clearly seen that the imaginary spectra intensity and lineshape evolve as a function of time, whereas in the real spectra, there is also time-dependent spectral evolution (Fig. 3b).

Because the spectral dynamics are clearly frequency-dependent (Fig. 3a), the integrated spectral dynamics can lose important insights. For example, even though there is a clear transient signal at long time delay, it appears the signal relaxes to zero in a few picoseconds in the transient imaginary spectral dynamics when integrated (Fig. 3b). To further extract dynamics of P3HT during interfacial charge transfer, we performed global analysis[40] on the real and imaginary parts of spectral dynamics, separately. The reconstructed HD tr-VSFG spectra from the global analysis results (Fig. 4a) well capture salient features of the experimental results, as indicated by the differences seen between experimental and reconstruction results (Fig. 4b).

Global analysis shows that both real and imaginary dynamics can be decomposed into three components (Fig. 5) that are simultaneous and parallel, rather than sequential. The lineshapes of the spectral components (Figs. 5a, b, and c) indicate that the spectral components are all dominated by NR signal except the imaginary part of component 3 (orange, Fig. 5c), which resembles the molecular spectral feature in static HD VSFG after phase rotation (Fig. 3c). What is particularly striking is that NR signals also

dominate imaginary spectral components 1 and 2, which is notable considering that NR signals have been removed from the imaginary VSFG spectra after phase rotation (Fig. 3c). This result indicates that upon photoexcitation, new NR signals, or a phase shift of NR signals, are created. However, it is interesting that even for NR signals, two different components are introduced. For example, the phases of transient components 1 and 2 are 2.94 and -1.59, respectively.

Another remarkable result is the agreement between the temporal dynamics of the real and imaginary components from the global analysis, despite the fact that the real and imaginary spectral dynamics are analyzed separately. Components 1, 2, and 3 have lifetimes c.a. 250 fs, 900 fs, and 40 ps, respectively, regardless of whether the component is from the real or imaginary spectral dynamics. This consistency implies that the real and imaginary parts of each component reflect the same physical process during interfacial charge transfer. Furthermore, we note the extracted lifetime for components 1 and 2 are very close to the lifetime of the phase dynamics fitted using Eq. 1, which indicates that the multi-exponential phase dynamics in Fig. 2d is composed of two parallel dynamical processes. Note that we only scan the dynamics to 7 ps, so the 40 ps lifetime only reflect and agree with the observation that there is a long

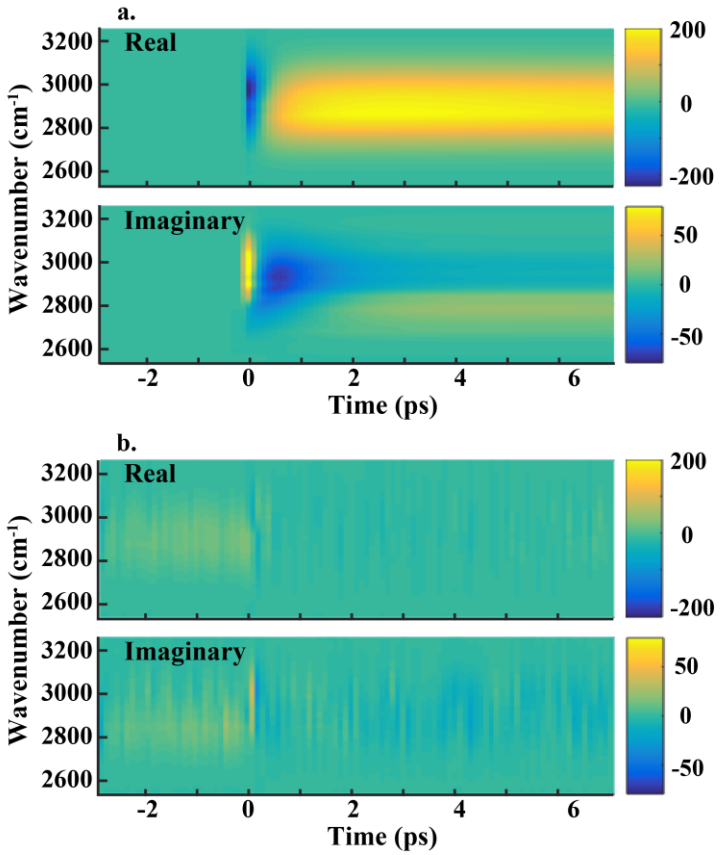

Figure 4. HD Transient-VSFG dynamics from global analysis. (a) Reconstructed real (upper panel) and imaginary (lower panel) 2D HD tr-VSFG spectrum of P3HT/Au from global analysis result. (b) The difference between the experimental and simulated 2D HD tr-VSFG spectrum, which shows good agreement.

dynamic component in the charge transfer process.

Based on the time-scale, we tentatively assign components 1 to be coherent artifacts and component 2 to be optical excitations that only lead to unsuccessful charge transfer which is fast charge recombination through hot electron scattering and electron – phonon scattering[15,41]. The ca. 250 fs relaxation time of

component 1 is just slightly longer than the instrumental response, but within the experimental uncertainty range. We note that components 1 and 2 together are likely to be the first component in our previous homodyne tr-VSFG work[15]. When homodyne detection is employed, it is difficult to disentangle the dynamical processes. With the additional phase measurement gained from heterodyne detection, these two dynamical processes are successfully disentangled. Thus, as a result, when homodyne detection was used, the relaxation dynamics was determined to be ca. 500 fs, which is likely to be convoluted results of the dynamics of coherent artifacts and charge relaxation[15]. Heterodyne detection provides a more accurate measurement for the charge recombination dynamics, which is ca. 900 fs.

Component 3 has a very long relaxation lifetime, matching with the direct interfacial charge transfer across the P3HT/Au interface, as we described before. It is interesting to note that the imaginary part of component 3 consists of purely resonant molecular signal, while the real part is dominated by NR signal. Nevertheless, both components have the same type of dynamics. This result suggests that both the molecule signal and the NR signal experience similar built-in electric fields upon charge transfer. This is consistent with the previous thoughts that electric-field-induced effect in charge transfer materials are dominated by NR signals[9]. However, we clearly show, using heterodyne detection, that molecular resonance features also have responses from electric-field-induced effect. The response is much smaller than the response from NR signals, but is not negligible and can only be learned with the help of HD detection. Most importantly, because we can now separate NR and molecular responses to local electric fields, and NR signal is mostly due to non-resonance electronic excitations, whereas molecular resonances represent local molecular excitations, this development augments local molecular sensitivity to build-in electrical fields. We include a cartoon (Fig. 5g) to better describe the physical process of dynamic component 2 and 3.

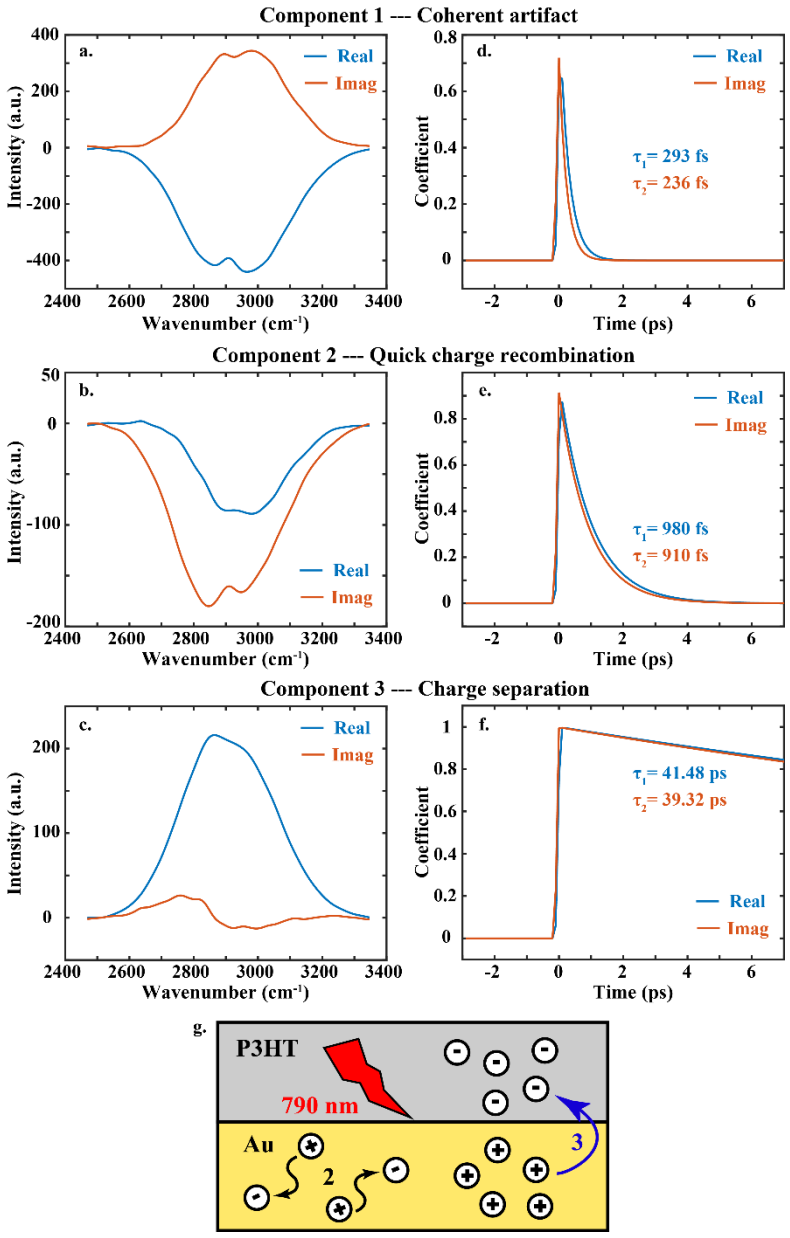

Figure 5. Individual plots of three different spectral components (a, b, and c) and their correspondent temporal coefficients (d, e, and f) from global analysis of the real part (blue) and imaginary part (red) of the spectrum. A schematic of dynamic component 2 and 3 is shown in g.

Conclusion

In this study, heterodyne detected transient electric-field-induced VSFG is demonstrated and applied to P3HT/Au interfaces. The heterodyne detection enables phase sensitivity in tracking electric-field-induced VSFG. Furthermore, to clearly resolve non-resonant and molecular resonant responses to local DC electric fields, we implemented a phase rotation scheme to rotate the non-resonant signal so that it only appears

at the real part of the VSFG spectra, which ensures the imaginary parts are composed purely of molecular resonance. The separation of non-resonance and molecular resonances in VSFG, along with its phase sensitivity, allowed us to resolve three spectral dynamic components. Using heterodyne detection, we successfully disentangled coherent artifacts and ultrafast dynamics of charge relaxation/recombination, which were convoluted in previous homodyne measurements. The third component resembled the direct charge transfer dynamics revealed in our previous homodyne measurements[15], which further supports the conclusion from our previous work that two types of charge dynamics, e.g., charge recombination and direct charge transfer, happen simultaneously at P3HT/Au interfaces.

Acknowledgments

This work was supported by National Science Foundation CHE-1808111. We appreciate Jiaxi Wang's contribution to the gold substrates preparation and Qiting Wu's help on the experiments. The sputtering was performed in Nano3 facility at UC, San Diego.

References

[1] W.A. Tisdale, K.J. Williams, B.A. Timp, D.J. Norris, E.S. Aydil, and X.-Y. Zhu, Science (80-.). **328**, 1543 (2010).

[2] R.D. Pensack and J.B. Asbury, J. Phys. Chem. Lett. **1**, 2255 (2010).

[3] G. Grancini, M. Biasiucci, R. Mastria, F. Scotognella, F. Tassone, D. Polli, G. Gigli, and G. Lanzani, J. Phys. Chem. Lett. **3**, 517 (2012).

[4] A.E. Jailaubekov, A.P. Willard, J.R. Tritsch, W.L. Chan, N. Sai, R. Gearba, L.G. Kaake, K.J. Williams, K. Leung, P.J. Rossky, and X.Y. Zhu, Nat. Mater. **12**, 66 (2013).

[5] K. Wu, J. Chen, J.R. McBride, and T. Lian, Science (80-.). **349**, 632 (2015).

[6] S.M. Falke, C.A. Rozzi, D. Brida, M. Maiuri, M. Amato, E. Sommer, A. De Sio, A. Rubio, G. Cerullo, E. Molinari, and C. Lienau, Science (80-.). **344**, 1001 (2014).

[7] W. Xiong, J.E. Laaser, P. Paoprasert, R.A. Franking, R.J. Hamers, P. Gopalan, and M.T. Zanni, J. Am. Chem. Soc. **131**, 18040 (2009).

[8] H. Zhu, J. Wang, Z. Gong, Y.D. Kim, J. Hone, and X.Y. Zhu, Nano Lett. **17**, 3591 (2017).

[9] T.C. Anglin, D.B. O'Brien, and A.M. Massari, J. Phys. Chem. C **114**, 17629 (2010).

[10] P. Dhar, P.P. Khlyabich, B. Burkhart, S.T. Roberts, S. Malyk, B.C. Thompson, and A. V. Benderskii, J. Phys. Chem. C **117**, 15213 (2013).

[11] Y. Li, J. Wang, and W. Xiong, J. Phys. Chem. C **119**, 28083 (2015).

[12] I. Yagi, K. Inokuma, K. Kimijima, and H. Notsu, J. Phys. Chem. C **118**, 26182 (2014).

[13] H. Vanselous and P.B. Petersen, J. Phys. Chem. C **120**, 8175 (2016).

[14] T.C. Anglin, Z. Sohrabpour, and A.M. Massari, J. Phys. Chem. C **115**, 20258 (2011).

[15] B. Xiang, Y. Li, C.H. Pham, F. Paesani, and W. Xiong, Sci. Adv. **3**, e1701508 (2017).

[16] R. Pandey, A.P. Moon, J.A. Bender, and S.T. Roberts, J. Phys. Chem. Lett. **7**, 1060 (2016).

[17] D.E. Gragson, B.M. McCarty, and G.L. Richmond, J. Am. Chem. Soc. **119**, 6144 (1997).

[18] Y. Li, J. Wang, M.L. Clark, C.P. Kubiak, and W. Xiong, Chem. Phys. Lett. **650**, 1 (2016).

[19] S. Nihonyanagi, T. Ishiyama, T. Lee, S. Yamaguchi, M. Bonn, A. Morita, and T. Tahara, J. Am. Chem. Soc. **133**, 16875 (2011).

[20] X. Chen, W. Hua, Z. Huang, and H.C. Allen, J. Am. Chem. Soc. **132**, 11336 (2010).

[21] C.H. Lee, R.K. Chang, and N. Bloembergen, Phys. Rev. Lett. **18**, 167 (1967).

[22] A.M. Darlington, T.A. Jarisz, E.L. Dewalt-Kerian, S. Roy, S. Kim, M.S. Azam, D.K. Hore, and J.M. Gibbs, J. Phys. Chem. C **121**, 20229 (2017).

[23] Y.-C. Wen, S. Zha, X. Liu, S. Yang, P. Guo, G. Shi, H. Fang, Y.R. Shen, and C. Tian, Phys. Rev. Lett. **116**, 016101 (2016).

[24] M. Doğangün, P.E. Ohno, D. Liang, A.C. McGeachy, A.G. Bé, N. Dalchand, T. Li, Q. Cui, and F.M. Geiger, J. Phys. Chem. B **122**, 4870 (2018).

[25] P.E. Ohno, H.F. Wang, F. Paesani, J.L. Skinner, and F.M. Geiger, J. Phys. Chem. A **122**, 4457 (2018).

[26] S.K. Reddy, R. Thiraux, B.A. Wellen Rudd, L. Lin, T. Adel, T. Joutsuka, F.M. Geiger, H.C. Allen, A. Morita, and F. Paesani, Chem **4**, 1629 (2018).

[27] S. Roy, C. Beutier, and D.K. Hore, J. Mol. Struct. **1161**, 403 (2018).

[28] S. Pezzotti, D.R. Galimberti, Y.R. Shen, and M.P. Gaigeot, Phys. Chem. Chem. Phys. **20**, 5190 (2018).

[29] T. Joutsuka and A. Morita, J. Phys. Chem. C **122**, 11407 (2018).

[30] S. Nihonyanagi, P.C. Singh, S. Yamaguchi, and T. Tahara, Bull. Chem. Soc. Jpn. **85**, 758 (2012).

[31] K. Matsuzaki, R. Kusaka, S. Nihonyanagi, S. Yamaguchi, T. Nagata, and T. Tahara, J. Am. Chem. Soc. **138**, 7551 (2016).

[32] C.C. Rich, K.A. Lindberg, and A.T. Krummel, J. Phys. Chem. Lett. **8**, 1331 (2017).

[33] P.C. Singh, S. Nihonyanagi, S. Yamaguchi, and T. Tahara, J. Chem. Phys. **137**, 094706 (2012).

[34] H. Wang, T. Gao, and W. Xiong, ACS Photonics **4**, 1839 (2017).

[35] A.R. Kannurpatti, J.W. Anseth, and C.N. Bowman, Polymer (Guildf). **39**, 2507 (1998).

[36] P. Pingel, A. Zen, R.D. Abellón, F.C. Grozema, L.D.A. Siebbeles, and D. Neher, Adv. Funct. Mater. **20**, 2286 (2010).

[37] W. Yang and D.K. Hore, J. Phys. Chem. C **121**, 28043 (2017).

[38] M. Fahlman, A. Crispin, X. Crispin, S.K.M. Henze, M.P. de Jong, W. Osikowicz, C. Tengstedt, and W.R. Salaneck, J. Phys. Condens. Matter **19**, 183202 (2007).

[39] J.E. Laaser, W. Xiong, and M.T. Zanni, J. Phys. Chem. B **115**, 2536 (2011).

[40] J.J. Snellenburg, S.P. Laptenok, R. Seger, K.M. Mullen, and I.H.M. van Stokkum, J. Stat. Softw. **49**, 1 (2012).

[41] M. V. Lebedev, O. V. Misochko, T. Dekorsy, and N. Georgiev, J. Exp. Theor. Phys. **100**, 272 (2005).